CHAPTER – 3

ONE-DIMENSIONAL PHOTONIC CRYSTAL COMPOSED OF EXPONENTIAL GRADED INDEX MATERIALS

3.1 Introduction

The discovery of photonic crystals (PCs) has triggered a growing interest in the study of the propagation of light through periodic structures which can be utilized in many branches of science and engineering. PCs forbid the propagation of electromagnetic waves in certain frequency ranges is called photonic band gap [Yablonovitch (1987); Joannopoulos (1997)]. Over the past several years, existence of photonic band gaps in 1-D PCs have been intensively investigated with different materials such as dielectric, anisotropic, negative refractive index, magnetic materials etc. in periodic and aperiodic structures [Tolmachev (2008); Alagappan (2006); Zharov (2008); Vasconcelos (2007); Yu (2007); Macia (2012); Ouyang (2008); Xiang (2010)].

Recently, graded photonic crystals (GPCs) and its optical properties have been the subject of great interest carried out in view of their fantastic applications such as spectral filters, high efficiency bending waveguides, couplers, beam aperture and deflector, super bending and self-focusing media, lenses, and antireflection coating, etc. [Wang (2011); Oner (2013); Cakmak (2009); Vasic (2011); Chhajed (2008)]. PCs with gradual variation of structural or material parameters in the direction perpendicular or normal to the propagation of electromagnetic waves are known as GPCs [Centeno (2005); Kurt (2007); Ren (2011); Rauh (2010); Sang (2006)]. Gradual variation of relative parameters in GPCs makes them very different from the conventional PCs regarding the performance.

In the previous chapter, the study of photonic band gap and defect modes properties in 1-D PCs composed of linear graded index materials has been presented. The importance of the tunable and controlled photonic band gap and defect modes in 1-D PCs with linear graded index materials has prompted us to extend the study on the photonic band gap and defect mode properties in the PCs with other types of graded index materials. In this chapter, we have presented the photonic and Omni-directional

band gaps and defect modes properties in 1-D PCs constituted with exponential graded index materials. Here, the refractive index in the graded materials layer varies exponentially as a function of the depth of layer. Initially, the theoretical models and calculation of the reflectance, transmittance and band structure of the structures with exponential graded index materials have presented. The effects of exponential graded index layers on the photonic and omnidirectional band gap and defect modes properties have discussed in the results and discussion section. The study has been carried out as follows. First, the reflection spectra and band structure of different layer thickness and various refractive index of the constituted normal layer have presented. Second, the omnidirectional band gap properties for the structures with quarter-wave and latent type layer stacking arrangements have investigated. Third, the effect of grading parameters on the photonic band gap in 1-D GPC structures has demonstrated. Next, transmission spectra and defect modes at different periodicity, defect layer thickness and grading parameter in the 1-D PC structure with a defect of exponential graded index material are demonstrated. Moreover, the effect of incident angle on the defect modes for transverse-electric (TE) and transverse-magnetic (TM) polarizations are also investigated. Finally, the results are briefly summarized.

3.2 Theoretical description

The schematic views of the considered 1-D GPC multilayer structures (Type1 and Type2) are shown in figure 3.1. The considered GPCs in our investigation are composed of two types of dielectric layers. One is the graded layer (A or A′) with exponentially varying refractive index as a function of the depth of layer and the other is homogeneous layer (B) with space independent refractive index. Type1 is the periodic structure of like $(AB)^N$ and Type2 is the periodic structure of like $(A'B)^N$, where N represents the number of periods. The widths of the graded and homogeneous layers are d_1 and d_2 respectively. Refractive index profile in the considered graded layers A and A′ varies in two different ways with depth of the graded layer. First, index of refraction increases exponentially from initial ($x = 0$) to the end ($x = d_1$) boundaries of the exponential graded index layer (A) and can be characterized as;

$$\boldsymbol{n(x) = n_i \exp\left(\frac{x}{d_1} \ln \frac{n_f}{n_i}\right)} \quad \ldots\ldots \quad \textbf{(3.1)}$$

Second, refractive index decreases exponentially from initial to final boundary in the exponential graded index (A′), which can be expressed as;

$$n(x) = n_f \exp\left(\frac{x}{d_1} \ln \frac{n_i}{n_f}\right) \quad \ldots\ldots \quad (3.2)$$

where n_i and n_f is the lower and higher index of refraction, respectively and d_1 is the layer thickness. Subscript i and f represent the lower and higher refractive index positions in the graded layers, respectively. In our proposed structures, first case is considered in layer A and second case in layer A′. The two representative structures of 1-D GPCs are a multilayer structures composed with layer A and A′, and their schematic diagram are illustrated in figure 3.1(a) and 3.1(b), respectively. Relative refractive index variations of the proposed structures are also shown in figure 3.1.

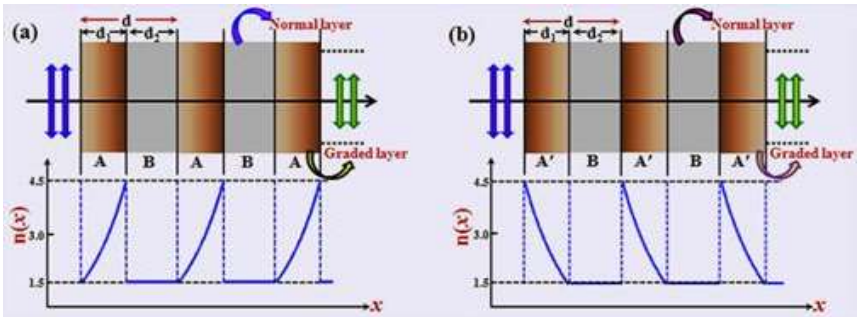

Figure 3.1 The schematic representation of the considered 1-D GPC structures composed of graded index materials with exponentially (a) increasing and (b) decreasing refractive index along the thickness of layer.

The wave equation for electromagnetic wave propagation in a graded index layer, which has exponentially varying refractive index along perpendicular (considered as x-direction) to the surface of graded layer can be written as;

$$\xi^2 \frac{d^2}{d\xi^2} E + \xi \frac{d}{d\xi} E + \frac{\xi^2}{\gamma^2} E = 0 \quad \ldots\ldots \quad (3.3)$$

where $\xi = \frac{2\pi}{\lambda} n(x)$ is the wave propagation vector for exponential graded index layers at normal angle of incidence. Refractive index $n(x)$ taken according the exponential graded index layers (A and A') with increasing and decreasing refractive index defined as equations (3.1) and (3.2), respectively and λ is the wavelength of light. Grading profile parameter for the exponentially graded index layers A and A' to be $\gamma = \frac{1}{d_1} \ln\left(\frac{n_f}{n_i}\right)$ and $\gamma' = \frac{1}{d_1} \ln\left(\frac{n_i}{n_f}\right)$, respectively. Therefore, the equations (3.1) and (3.2) for the variations of refractive index in the exponential graded index layers A and A′ can be represented as $n(x) = n_i e^{\gamma x}$ and $n(x) = n_f e^{\gamma' x}$, respectively [Yeh (1988)].

The solution of equation (3.3) can be expressed for increasing refractive index in the exponential graded layers as;

$$E(x) = A_E J_0\left(\frac{\xi}{\gamma}\right) + B_E Y_0\left(\frac{\xi}{\gamma}\right) \quad \ldots\ldots \quad (3.4)$$

where A_G and B_G are arbitrary constants for the graded layers, J_0 and Y_0 are first and second kind of 0^{th}-order Bessel function, respectively. Subscript E represents for an exponential graded index layer. Similarly, the solution for exponential graded index layer with decreasing refractive index to be similar as equation (3.4), but propagation wave vector and grading profile parameter change according to this layer. The distribution of electric field along the direction of wave propagation in a dielectric homogeneous layer can be written as:

$$E(x) = A_H e^{-i\,k_H\,x} + B_H e^{i\,k_H\,x} \quad \ldots\ldots \quad (3.5)$$

where A_H and B_H are the arbitrary constants, k_H is the wave vector and at normal angle of incidence $k_H = (2\pi/\lambda)n_B$. Subscript H represents for a homogeneous layer.

Multilayer interface optics and dispersion relation of the multilayered structures are obtained by solving the electromagnetic wave equation of layers in the multilayer structures. It can be described as the use of the amplitudes and phases of light reflected (or transmitted) at material boundaries to produce interference effects. So the components of the electric and magnetic fields within the layers of the multilayer structures can easily deduce. The expression of the electric fields, which is perpendicular to the incidence plane, in each one of the slabs in the periodic structure $(AB)^N$ can be expressed as;

$$E(x) = \begin{cases} A_0\, e^{-ik_0 x} + B_0\, e^{ik_0 x}, & x \le x_0 \\ \left[A_1 J_0\left(\frac{\xi}{\gamma}\right)_{(x-x_0)} + B_1 Y_0\left(\frac{\xi}{\gamma}\right)_{(x-x_0)}\right], & x_0 \le x \le x_1 \\ A_2\, e^{-ik_H(x-x_1)} + B_2\, e^{ik_H(x-x_1)}, & x_1 \le x \le x_2 \\ \left[A_3 J_0\left(\frac{\xi}{\gamma}\right)_{(x-x_2)} + B_3 Y_0\left(\frac{\xi}{\gamma}\right)_{(x-x_2)}\right], & x_2 \le x \le x_3 \\ \ldots\ldots\ldots & \ldots\ldots\ldots \\ \ldots\ldots\ldots & \ldots\ldots\ldots \\ A_{2n}\, e^{-ik_H(x-x_{2n-1})} + B_{2n}\, e^{ik_H(x-x_{2n-1})}, & x_{2n-1} \le x \le x_{2n} \\ A_{2n+1}\, e^{-ik_0(x-x_{2n})}, & x_{2n} \le x \end{cases} \quad \ldots\ldots \quad (3.6)$$

with

$$x_0 = 0, x_1 = d_1,$$
$$x_2 = x_1 + d_2 = d_1 + d_2 = d,$$
$$x_3 = x_2 + x_1 = d_1 + d_2 + d_1 = d + d_1,$$
$$\ldots\ldots\ldots$$
$$x_{2n-1} = (N-1)d + d_1,$$
$$x_{2n} = Nd,$$
$$N = 2n.$$

where k_0, k_H and ξ are the wave vectors in air, homogeneous and graded index media, respectively, n represents the n^{th} media and N is the number of periods. In the considered media, the electric field is taken to be the sum of a propagating and a counter-propagating wave with similar wave vectors but opposite direction and their amplitudes given by the coefficients labelled as A_l and B_l (l = 0, 1, 2 …2n+1), respectively. Similarly, the expression for the electric field in each one of the slabs in the periodic structure $(A'B)^N$ can be written as above equations, only the propagation wave vector and grading profile parameter changes according to the layer A'.

To calculate the reflectance (R) and transmittance (T), it is necessary to calculate the reflection and transmission coefficients of the fields in incident and outgoing media, labeled as r and t respectively due to partially transmitted and reflected waves generated at each interface in multilayer structures. The reflection and transmission coefficients of each layer of the multilayer structures are represented as the frequency dependent coefficients A_l and B_l ($l = 1, 2, 3 \ldots$), respectively. In case of TE-polarization, the frequency dependent coefficients A_l and B_l are determined by imposing the continuity conditions for both electric and magnetic fields across the interface from one medium to the other, which establishes a set of equations for the transfer matrix formalism. The set of equations are expressed as:

$$\underbrace{\begin{pmatrix} 1 & 1 \\ ik_0 & -ik_0 \end{pmatrix}}_{M_0}\begin{pmatrix} A_0 \\ B_0 \end{pmatrix} = \underbrace{\begin{pmatrix} J_0\left(\frac{\xi_0}{\gamma}\right) & Y_0\left(\frac{\xi_0}{\gamma}\right) \\ \xi_0 J_1\left(\frac{\xi_0}{\gamma}\right) & \xi_0 Y_1\left(\frac{\xi_0}{\gamma}\right) \end{pmatrix}}_{M_l}\begin{pmatrix} A_1 \\ B_1 \end{pmatrix}$$

$$\underbrace{\begin{pmatrix} J_0\left(\frac{\xi_1}{\gamma}\right) & Y_0\left(\frac{\xi_1}{\gamma}\right) \\ \xi_1 J_1\left(\frac{\xi_1}{\gamma}\right) & \xi_1 Y_1\left(\frac{\xi_1}{\gamma}\right) \end{pmatrix}}_{M_f}\begin{pmatrix} A_1 \\ B_1 \end{pmatrix} = \underbrace{\begin{pmatrix} 1 & 1 \\ ik_H & -ik_H \end{pmatrix}}_{M_1}\begin{pmatrix} A_2 \\ B_2 \end{pmatrix}$$

$$\underbrace{\begin{pmatrix} e^{-ik_H d_2} & e^{ik_H d_2} \\ ik_0 e^{-ik_H d_2} & -ik_0 e^{ik_H d_2} \end{pmatrix}}_{M_2}\begin{pmatrix} A_2 \\ B_2 \end{pmatrix} = \underbrace{\begin{pmatrix} J_0\left(\frac{\xi_0}{\gamma}\right) & Y_0\left(\frac{\xi_0}{\gamma}\right) \\ \xi_0 J_1\left(\frac{\xi_0}{\gamma}\right) & \xi_0 Y_1\left(\frac{\xi_0}{\gamma}\right) \end{pmatrix}}_{M_i}\begin{pmatrix} A_3 \\ B_3 \end{pmatrix}$$

… … … so on

… … (3.7)

where $k_0 (= (2\pi/\lambda).n_0.cos\theta_0)$ and $k_H (= (2\pi/\lambda).n_H.cos\theta_H)$ are the wave vectors of the incident (0^{th}) and homogeneous media, respectively. n_0 and θ_0 are refractive index and incident angle of the air (0^{th}) media, n_H and θ_H are refractive index and incident angle of the homogeneous media, respectively. In case of the graded layers, wave

vectors at boundary of lower and higher refractive indices are $\xi_0 = \omega.n_i.cos\theta_i/c$ and $\xi_1 = \omega.n_f.cos\theta_f/c$, where θ_i and θ_f are angle of incidence at boundary of lower (n_i) and higher (n_f) refractive index of the graded layer, respectively.

The expressions of the set of equations across the interface from one medium to the other are similar for both structures (Type1 and Type2) but their characteristic matrices will change due to the variation of refractive index in the graded layer. In case of exponentially increasing refractive index layers, wave vectors at initial and final boundaries are $\xi_0 = \omega.n_i.cos\theta_i/c$ and $\xi_1 = \omega.n_f.cos\theta_f/c$, while the wave vectors at initial and final boundaries for exponentially decreasing refractive index layers become $\xi_1 = \omega.n_f.cos\theta_f/c$ and $\xi_0 = \omega.n_i.cos\theta_i/c$, respectively. Here, n_f and n_i are refractive index at initial and final boundary of the graded layers, respectively.

To investigate the propagation properties of the electromagnetic wave in the periodic structures $(AB)^N$ and $(A'B)^N$, the transfer matrix method have embraced and calculated the reflectance and photonic band gap spectra. After applying the transfer matrix approach on the considered structures, the electromagnetic wave propagation through the considered structures $(AB)^N$ can be expressed by multiplying the characteristic matrices of the constituent layers (A and B) as;

$$\begin{pmatrix} \boldsymbol{A_0} \\ \boldsymbol{B_0} \end{pmatrix} = \boldsymbol{M_0^{-1}}.(\boldsymbol{M_G}.\boldsymbol{M_H})^N.\boldsymbol{M_0}\begin{pmatrix} \boldsymbol{A_{N+1}} \\ \boldsymbol{0} \end{pmatrix} \quad \ldots\ldots \quad \textbf{(3.8)}$$

Similarly, the electromagnetic waves propagation through the considered structures $(A'B)^N$ can be expressed by multiplying the characteristic matrices of constituent layers (A′ and B) as:

$$\begin{pmatrix} \boldsymbol{A_0} \\ \boldsymbol{B_0} \end{pmatrix} = \boldsymbol{M_0^{-1}}.(\boldsymbol{M'_G}.\boldsymbol{M_H})^N.\boldsymbol{M_0}\begin{pmatrix} \boldsymbol{A_{N+1}} \\ \boldsymbol{0} \end{pmatrix} \quad \ldots\ldots \quad \textbf{(3.9)}$$

where N is the number of the periods, A_0, B_0 and A_{N+1} are the arbitrary constant for incident (0^{th}) media and outgoing $(N+1)^{th}$ media, respectively. Matrix M_G and M'_G are the characteristics matrix of the exponentially graded index layers A and A', respectively. Matrix M_H and M_0 is the characteristics matrix of homogeneous layers and air media, respectively. The characteristic matrices are $M_G = M_i.{M_f}^{-1}$, $M_H = M_1.{M_2}^{-1}$ and $M'_G = M_f.{M_i}^{-1}$, where M_i and M_f are characteristic matrices at lower and higher refractive index boundaries of the graded layers, $M_1$and M_2 are characteristic matrices at the initial and final boundaries of the normal layers, as given in a set of equations for the interface from one medium to the other, respectively.

Now, 1-D PC structure containing a defect layer of an exponential graded index material is considered. A schematic view of the structure with doping of a defect layer of an exponential graded index material is shown in the panel (a) of the figure 3.2, which composes a system of the form $(AB)^P ADA(BA)^P$, where P is the periodicity of the unit cells. The proposed 1-D PC is composed of two types of dielectric homogeneous layers and an exponential graded index layer as defect. Here, dielectric layers are represented as A and B, and a defect layer is considered as D. The relative refractive index of the layers A and B are assuming as n_A and n_B, and equal to 1.5 and 4.5, respectively. The defect layer D, which generates defect modes inside the photonic band gaps has been considered of an exponential graded index material. The refractive index in the graded layer varies with the depth of layer. The schematic view of the variations of the refractive index of the central unit cells is depicted in panel (b) of the figure 3.2. The refractive index of the graded layer varies only in x-direction. The thickness of layers A, B and D are assume to be a, b and d, respectively.

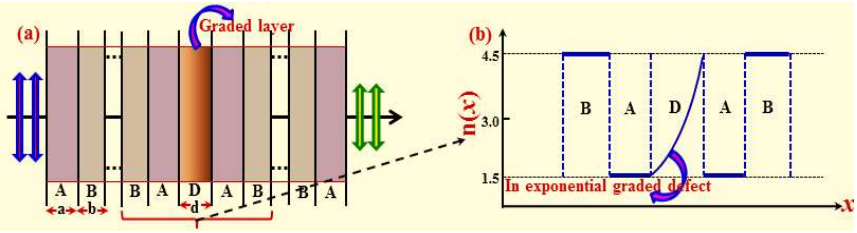

Figure 3.2 (a) Schematic representation of the 1-D PC structure with defect layer (D) as an exponential graded material of the form $(AB)^P ADA(BA)^P$ with period P and panel (b) show the relative refractive index variation in central unit cells.

Applying the transfer matrix approach, the amplitudes A_0 and B_0 of the electromagnetic field in the air medium at $x<0$ are related to the amplitudes A_{n+1} and B_{n+1} of the $(n+1)^{th}$ medium through the linear matrix transformation. Therefore, for the multilayer structures, the total transfer matrix equation can be written as;

$$\begin{pmatrix} A_0 \\ B_0 \end{pmatrix} = M_{i,j} \cdot \begin{pmatrix} A_{n+1} \\ B_{n+1} \end{pmatrix} \qquad \ldots\ldots \qquad (3.10)$$

where $M_{i,j}$ $(i, j = 1,2)$ is the total characteristic matrix and if atmosphere around the system is air, $M_{i,j} = M_0^{-1} . (M_1 \times M_2 \times M_3 \ldots \times M_n) . M_0$ for the n layer system and M_n is the characteristic matrix of n^{th} layer. Layers may be homogenous materials or exponential graded materials.

If the electric field is known at the beginning of the system, the field at the end of the same system can be derived from a simple matrix operation as given in the above

groups of equation according to the considered multilayer structures. The mathematical expression of the stacking of layers can then be represented as a complete system matrix. In this way, the reflection (r) and transmission (t) coefficients of the fields in the incident and outgoing media can be directly obtained. So, the reflectance (R) and transmittance (T) of the structures are determined using the following relations:

$$\boldsymbol{R = |r|^2 = \left|\frac{B_0}{A_0}\right|^2} \text{ and } \quad \boldsymbol{T = |t|^2 = \left|\frac{A_{N+1}}{A_0}\right|^2} \quad \text{… …} \quad \textbf{(3.11)}$$

A periodic layer structure is equivalent to a one-dimensional lattice that is invariant under the lattice translation. Here, refractive indices of layers are unchanged by the translation of the wave vector by a lattice constant d, where d is the total thickness of the periodic system. Using the Floquet's theorem, the solution of the wave equation of a period of the electric field for a periodic layer system as shown in figure 3.1 can be written as $E_K(x,z) = E_K(x) \,.\, e^{-i.\beta.z - i.K.x}$, where E_K is periodic with period d, i.e. $E_K(x+d) = E_K(x)$ and constant K is known as the Bloch wave number. Hence the dispersion relation for a periodic layer medium can be written as;

$$\boldsymbol{\cos\big(d.K(\beta,\omega)\big) = \frac{1}{2}\,(M_{11} + M_{22})} \quad \text{… …} \quad \textbf{(3.12)}$$

where d (= d_1+d_2) is the total thickness of a period of the periodic system, M_{11} and M_{22} are the diagonal elements of the 2x2 translation matrix $M_{ij}(i,j = 1,2)$. Here, optical transfer matrix (M_{ij}) of a period equal to $M_G.M_H$ and $M'_G.M_H$ for the considered structures with exponentially increasing and decreasing of the refractive index between the boundaries of the exponential graded index layer, respectively. The dispersion relation exhibits multiple spectral bands classified into two regimes. First, spectral band which in K is real correspond to propagating modes. Defined by the condition $|(M_{11} + M_{22})/2| \leq 1$, these bands are numbered as 1, 2, 3…, starting with the lowest-frequency band. Second, spectral band within which K is complex correspond to evanescent waves that are rapidly attenuated. Defined by the condition $|(M_{11} + M_{22})/2| > 1$, these bands correspond to the stop bands. They are also called photonic band gaps (PBG) or forbidden gaps since propagating modes do not exist [Yeh (1988)].

3.3 Numerical results and discussion

In this section, some numerical results to characterize the optical reflection, band structures, phase shift, photonic and omnidirectional band gaps and defect modes due to

the relevant structural parameters of considered 1-D GPC structures have presented. First, the optical properties of the periodic structures with exponential graded index materials as shown in figure 3.1 are studied. The medium B consider as homogeneous layer with variable refractive index n_B, while medium A or A' (Graded layer) has exponentially varying refractive index with depth of layer in increasing (for layer A) and decreasing (for layer A') fashion between lower refractive index, $n_i = 1.5$ and higher refractive index, $n_f = 4.5$, as expressed by equation (3.1) and (3.2), respectively. In this study, it assumes that light incident through the air medium and materials are lossless dielectric. Second, the photonic band gap and defect mode properties in the 1-D PC structure with a defect layer of exponential graded index material are investigated. Our results observation for the considered 1-D PC structures constituting exponentially graded index layers have been carried out in the following parts.

3.3.1 **Effect of layer thickness on photonic band gaps**

Initially, the reflection spectra of the structures at different layer thickness for some selected refractive index of homogeneous layer B under normal incident angle have presented. Thickness of a homogeneous and graded layers are chosen as to give; $n_G d_1 = n_B d_2 = D$, where d_1 and d_2 are the thickness of the graded and homogeneous layer, respectively and n_G is the mean value of the initial (n_i) and final (n_f) refractive index of the graded layer. For various layer thickness, D considered as $q\lambda_0/4$ (q = 1, 2, 3 … so on), where λ_0 is the optical wavelength equal to the wavelength for the mean value (450 THz) of the considered frequency region (150 - 750 THz). As is evident from the results shown in figure 3.3, there exists number of photonic bands, where electromagnetic waves cannot be transmitted. The number of photonic bands increases with increasing the thickness of layers for different considered refractive index of the homogeneous layer B. Because, the rate of change of refractive index in graded layers and contrast of the refractive index of the constitute layers increases with increasing the thickness of layers, and the average refractive index over the volume of each graded layer becomes large. Hence, influence the Bragg stack become more effectively. Formation of reflection spectra is same for the structures with exponential graded layer A or A′. Figures 3.3(a), 3.3(b) and 3.3(c), respectively show the reflection spectra of the considered structures for constituted homogeneous layer refractive index n_B equal to 2.0, 1.5 and 1.0. For all the considered refractive index of the homogeneous layer B, formation of photonic bands is similar under normal angle of incidence, but the

bandwidth of photonic bands is different. Bandwidths are larger for n_B equal to 1.0 as compare to other n_B values. Bandwidth of photonic bands decreases with increase of the n_B values because the photonic band gap properties are basically affected by the contrast of refractive index of constituted media. Contrast of refractive index of homogeneous layer and graded layer is higher for n_B equal to 1.0 as compare to other considered values, therefore the Bragg stack is more effectively and widths of photonic bands are large.

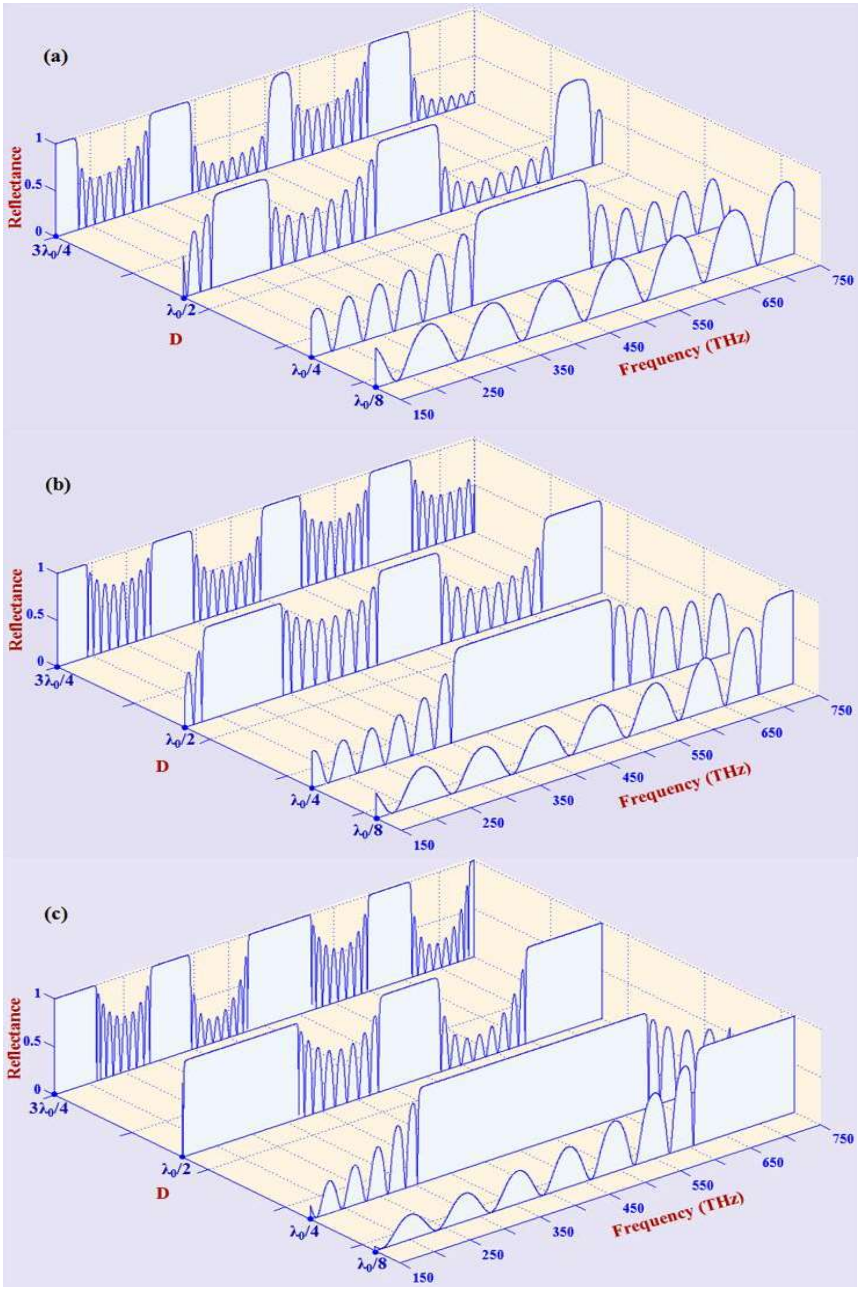

Figure 3.3 Reflectance spectra of the structures for the refractive index (a) $\boldsymbol{n_B = 2.0}$, (b) $\boldsymbol{n_B = 1.5}$ and (c) $\boldsymbol{n_B = 1.0}$, with various layer thickness constant D.

Now, the confinement effects arising from competition between the structures induced by changing the thickness of layers and magnitude of the total photonic bandwidths have examined. To do that, we calculate the regions for forbidden frequencies (stop bands), where $|(M_{11} + M_{22})/2| > 1$, as a function of the thickness of the layers is depicted in figure 3.4(a) and 3.4(b) for the structures with various refractive index of homogeneous layer n_B equal to 1.0 and 1.5, respectively. These figures show the distribution of the forbidden (black region) and allowed (white region) frequencies as a function of the thickness of layers for the structures with n_B equal to 1.0 and 1.5 up to the value of D equal to $9\lambda_0/4$. Note that, as expected for large layer thickness, the number of forbidden bands obtains and their bandwidths become narrower and narrower as an indication of more photonic band gaps with small bandwidths. The number of photonic bands are approximate same for the structures with acceptable n_B-values but their bandwidths are different.

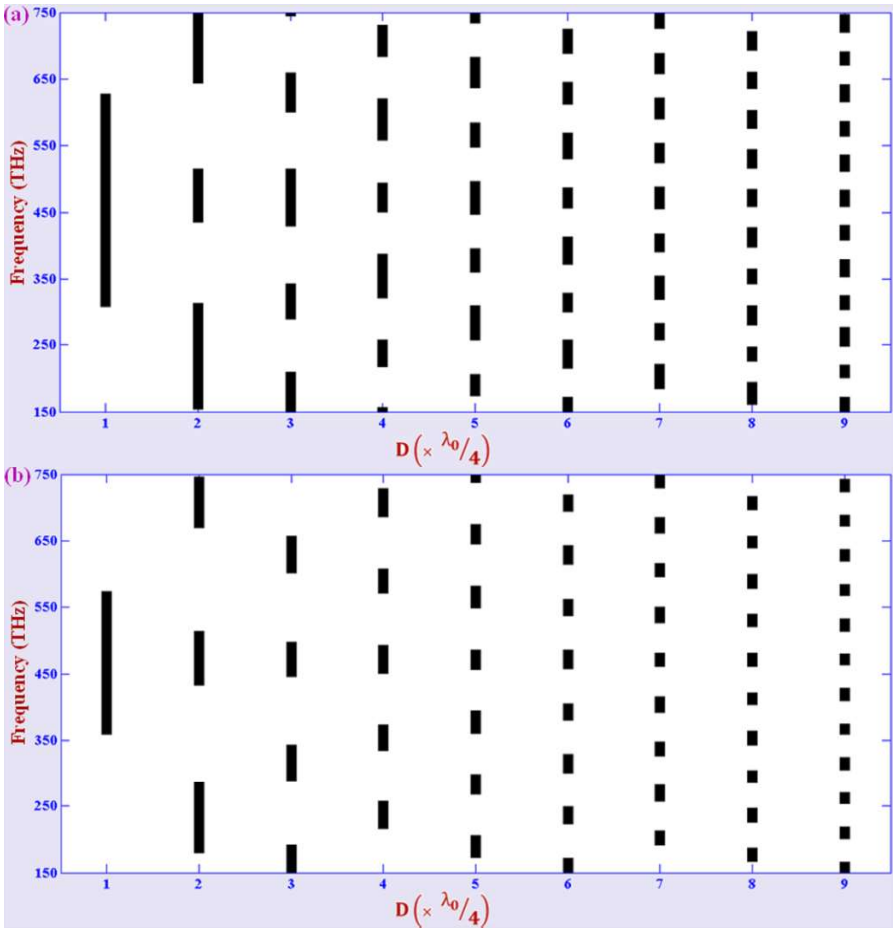

Figure 3.4 The distribution of photonic bandwidths as a function of the layer thickness constant D (= $q\lambda_0/4$, q = 1, 2, 3 …) for the structures with homogenous layer refractive index (a) $\boldsymbol{n_B}$ = 1.0 and (b) $\boldsymbol{n_B}$ = 1.5.

Total bandwidths for the structures with n_B equal to 1.0 are maximum as compare to other, which is clearly demonstrated in figure 3.5. This figure show the variation of the total band gap as the function of layer thickness constant (D) up to the value of D equal to $9\lambda_0/4$ for the structures with various refractive index n_B. It reveals that the total band gaps randomly change with increasing the layer thickness, but it is extremun for the structures with latent type layer stacking arrangements.

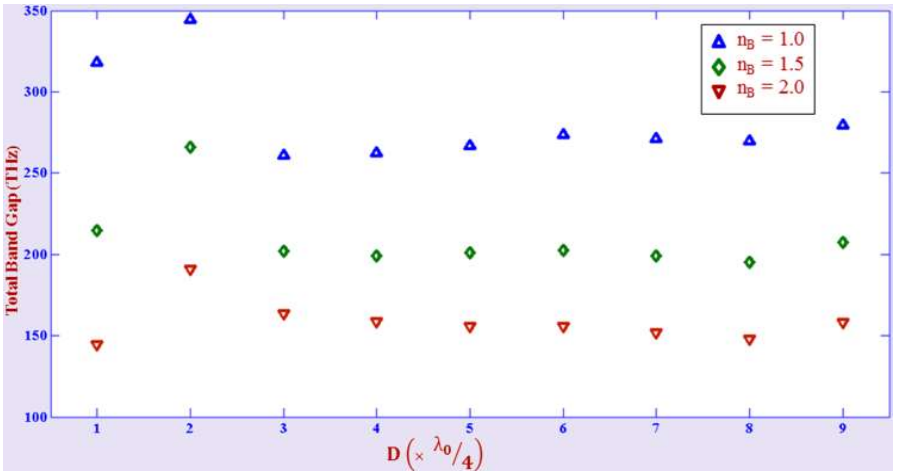

Figure 3.5 The distribution of total band gap of the photonic band gaps against the layer thickness constant D (= $q\lambda_0/4$, where q = 1, 2, 3 …).

Furthermore, we have emphasized the PBGs as changing of the refractive index of the normal layer B. To do that, we have calculated the regions for forbidden (stop bands) frequencies, where $|(M_{11} + M_{22})/2| > 1$, as a function of n_B is shown in figure 3.6(a) and 3.6(b), respectively for the structures with quarter wave arrangements and precise layer thickness d_1 = 50 nm and d_2 = 75 nm. These figures show the distribution of the forbidden (black region) and allowed (white region) frequencies region as a function of n_B up to the value equal to 4.5. As shown in figure 3.6(a), the PBG initially decreases with increasing the value of n_B up to 3.0 and then slowly increases for higher value of n_B in the structures with quarter wave layer arrangements, while for the structure with precise layer thickness d_1 = 50 nm and d_2 = 75 nm, behavior of PBGs variation is same as above but it shifted toward lower frequency region with increasing the value n_B as depicted in figure 3.6(b). Note that new PBGs are also generated at higher values of n_B for the structure with precise layer thickness. Here, it can also see that the values of n_B in the structures with quarter wave layer arrangements only influence on the bandwidth of PBGs, while for the structures with precise layer thicknesses, the values of n_B influence on both bandwidth and generation of new PBGs.

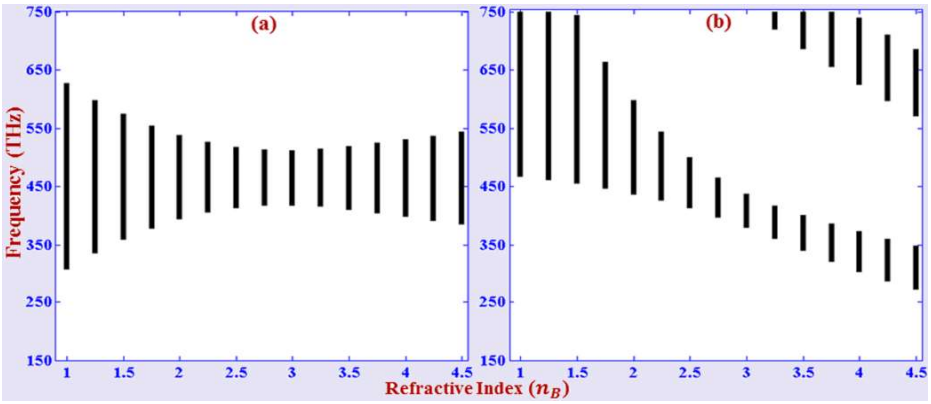

Figure 3.6 The distribution of photonic bandwidths as a function of the homogenous layer refractive index n_B for the structures with (a) quarter wave layer stacking arrangement and (b) precise layer thickness d_1 = 50 nm and d_2 = 75 nm arrangement.

For better understanding the effect of graded layer in the considered 1-D GPCs, we have calculated the spatial distribution of the square magnitude of the electric field for three selected frequencies impinging under ≈0%, ≈50% and ≈100% reflection conditions for the structures $(AB)^{10}$ and $(A'B)^{10}$, and demonstrated in figure 3.7. The electric field is denoted by E(x). For the sake of clarity, we have chosen the thickness of layers with relative refractive index equal to $5\lambda_0/4$ for better appreciated of the variations of electric fields. From the reflection spectra of the structures with n_B equal to 1.0, it can be observed that at the spectral band edge positions 635 THz, where close to 0% reflection is found, reflection is maximum ≈100% within the band gap region that observed for a frequency 580 THz inside the band gap, and for one of the reflection peak at 628.4 THz where ≈50% reflection is observed. Therefore, the distribution of the electric field intensity within the considered structures for frequencies 635 THz, 628.4 THz and 580 THz is demonstrated in figure 3.7(a), 3.7(b) and 3.7(c), respectively. Panels (i) and (ii) of the figure 3.7 show the distribution of electric field intensity in the periodic structures $(AB)^{10}$ and $(A'B)^{10}$, respectively. It can see that the electric field distributions in exponential graded layers for different grading profiles are quite different, although the volume-average refractive index is same. For the graded layers with exponentially increasing refractive index profile, the electric field intensities in exponential graded layers decrease as propagating depth increases as seen in panels (i) of the figure 3.7, while intensities increase with increases propagating depth in the graded layers for exponential decreasing refractive index profile as depicted in panels (ii) of the figure 3.7. The reason is the effect of inhomogeneity in the exponential graded layers. The variations of electric field intensities in graded layers change due to

the space dispersive refractive index in increasing and decreasing fashion as a function of the graded layer depth. On the other hand, the electric field intensities in non-graded layers keep unchanged in both types of periodic structures $(AB)^{10}$ and $(A'B)^{10}$.

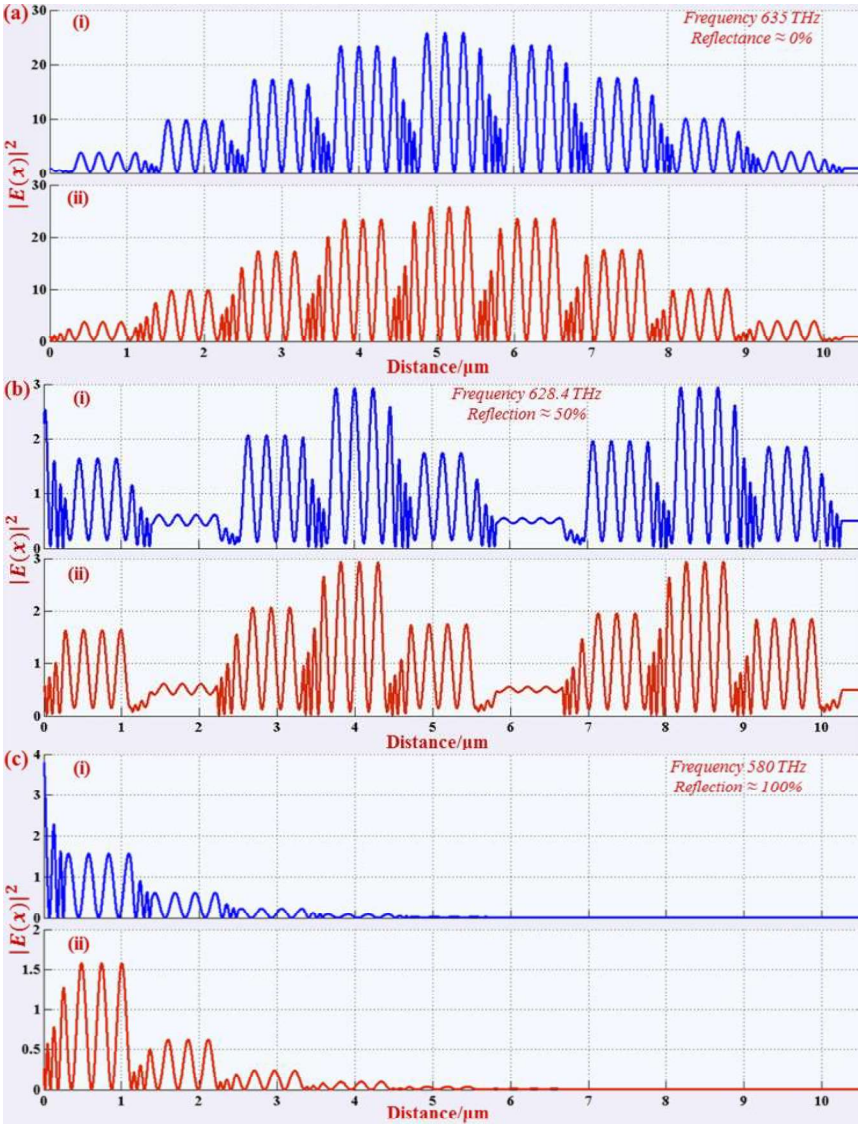

Figure 3.7 Panels (i) and (ii), respectively show the spatial distributions of the electric field intensity in the systems type1 $(AB)^{10}$ and type2 $(A'B)^{10}$ at three selected frequencies (a) 580 THz, (b) 628.4 THz and (c) 635 THz, impinging under ≈0%, ≈50% and ≈100%, respectively.

Due to the importance of the widespread photonic band gaps in 1-D GPCs, we would like to extend the study on the dispersion curves and reflection phase shift associated with the wider PBGs in the structures with $n_B = 1.0$. For different layer thickness, dispersion curves are calculated from equation (3.12) for the unbounded periodic structures and shown in panels (i) of the figure 3.8 as functions of the reduced

Bloch wave vector kd/π, and related reflection phase shifts are likewise illustrated in panels (ii) of the figure 3.8. As expected, the band gaps observed at zero transmission intensity range. The corresponding dispersion curves for the finite crystal are depicted in panels (i) of the figures 3.8 (a) and 3.8(b), respectively for layer thickness with relative refractive index proportional to $\lambda_0/4$ and $\lambda_0/2$. Also as seen here, the number of photonic bands increases with increase in layer thickness, single band formed for layer thickness with relative refractive index equal to $\lambda_0/4$ and three bands for $\lambda_0/2$, but the bandwidths become narrow and narrow with increase the number of photonic bands.

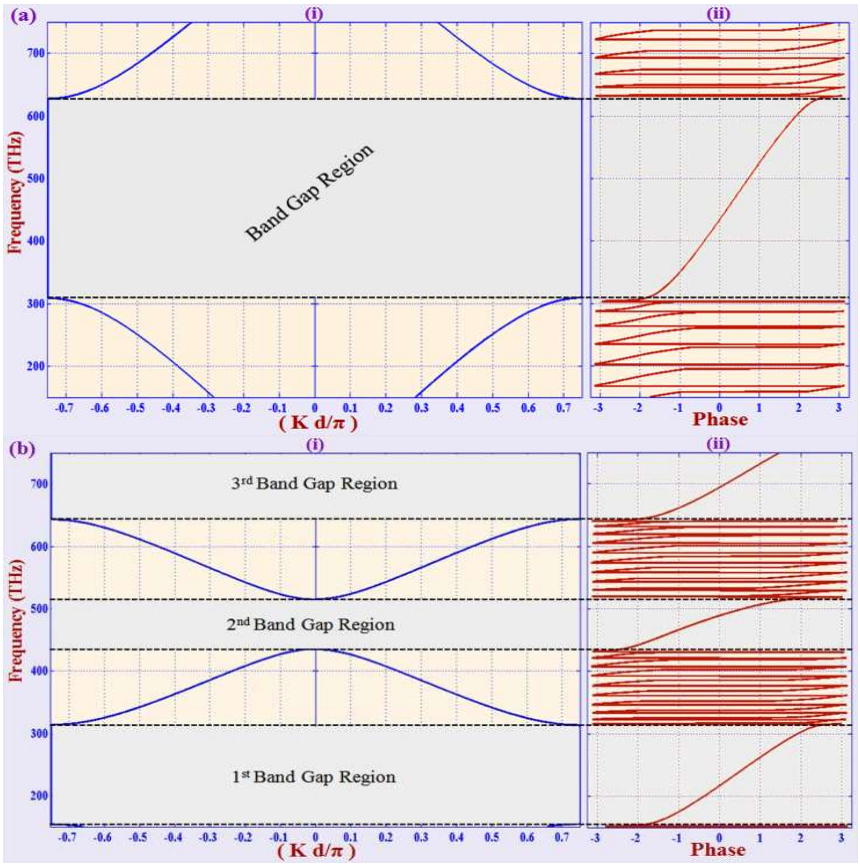

Figure 3.8 Panels (i) and (ii), respectively show the dispersion spectra and phase shifts of the considered structures for optical layer thicknesses with relative refractive index equal to (a) $\lambda_0/4$ and (b) $\lambda_0/2$.

Moreover, we observe that the reflection phase shifts varies from close to $-\pi$ at one band edge to approximate π at another band edge of the stop bands for the precise arrangement of unit cells in structures as seen in panels (ii) of the figure 3.8. Here, we have investigated reflection phase shifts for one of the specified possible arrangements of layers in period 'BA' of the considered graded photonic crystal structures. For other periodic arrangements such as AB or A'B or BA', reflection phase shifts varies in

different ways between –π at one band edge to +π at another band edge of the stop bands. The explanation for this phenomenon is that, in the stop band, the electric field of the lower band edge is mainly distributed in the non-graded material of the unit cell, while distribution of electric field in graded layer have adequate amplitudes at the upper band edge. In graded layers, distribution of field changes according to the gradation profiles. Therefore, due to the transform of field intensities distribution at the interface boundaries, the phase shifts are change between +π and –π with different values.

According to our results, we observe that reflection, transmission and photonic band gap spectra are independent on the arrangement of graded layers (A or A') in unit cells of the structures, whereas field distributions and reflection phase shifts change with arrangement of graded layers in unit cells of the structures. The forbidden bands region and bandwidths of the structures for different layer thicknesses and various refractive index of the homogeneous layer B are listed in Table 3.1.

Table 3.1 Reflection bands region and bandwidths in the 1-D GPC structures at normal incidence for different layer thickness.

Layer thickness constant (D)	Structures with $n_B = 2.0$		Structures with $n_B = 1.5$		Structures with $n_B = 1.0$	
	Reflection Band Region (nm)	Reflection Bandwidth (nm)	Reflection Band Region (nm)	Reflection Bandwidth (nm)	Reflection Band Region (nm)	Reflection Bandwidth (nm)
$\lambda_0/8$	…….	……	750.0 – 719.0	31	750.0 – 617.8	132.2
$\lambda_0/4$	538.0 – 393.8	144.2	574.0 – 359.6	214.4	627.0 – 309.0	318
$\lambda_0/2$	269.0 – 197.0	72	287.0 – 179.8	107.2	313.4 – 154.6	158.8
	512.2 – 431.2	81	514.0 – 432.6	81.4	514.8 – 435.4	79.4
	725.8 – 688.4	37.4	746.2 – 669.2	77	750.0 – 643.6	106.4
$3\lambda_0/4$	179.2 – 150.0	29.2	191.2 – 150.0	41.2	209.0 – 150.0	59
	341.8 – 287.6	54.2	342.4 – 289.2	53.2	343.2 – 290.2	53
	483.8 – 459.0	24.8	497.4 – 446.2	51.2	515.6 – 429.2	86.4
	655.8 – 601.0	54.8	656.6 – 601.2	55.4	658.6 – 601.0	57.6
					750.0 – 745.0	5

Now, to have a more complete description and a better understanding of the effect of the layer thickness on the PBG properties, it is important to know how layer thicknesses change the properties of the reflection and PBG for the structures with specific layer widths. The reflection spectra for different layer thicknesses of graded layers (d_1) and normal layers (d_2) are shown in figure 3.9(a) and 3.9(b) for the structures with fixed values of d_2 = 75 nm and d_1 = 50 nm, respectively. The acquired band gap is

shifted towards the lower frequency region and their bandwidth also decreases with increasing the values of thickness d_1 and d_2, which is clearly demonstrated in figure 3.9(a) and 3.9(b), respectively. Note that, as expected for large layer thickness, new forbidden bands generates because contrast of effective refractive index in the structure increases with increasing the thickness of layers. The change of exponential graded index layers thickness has great influence on the formation of PBGs as compare to the change of normal layers thicknesses.

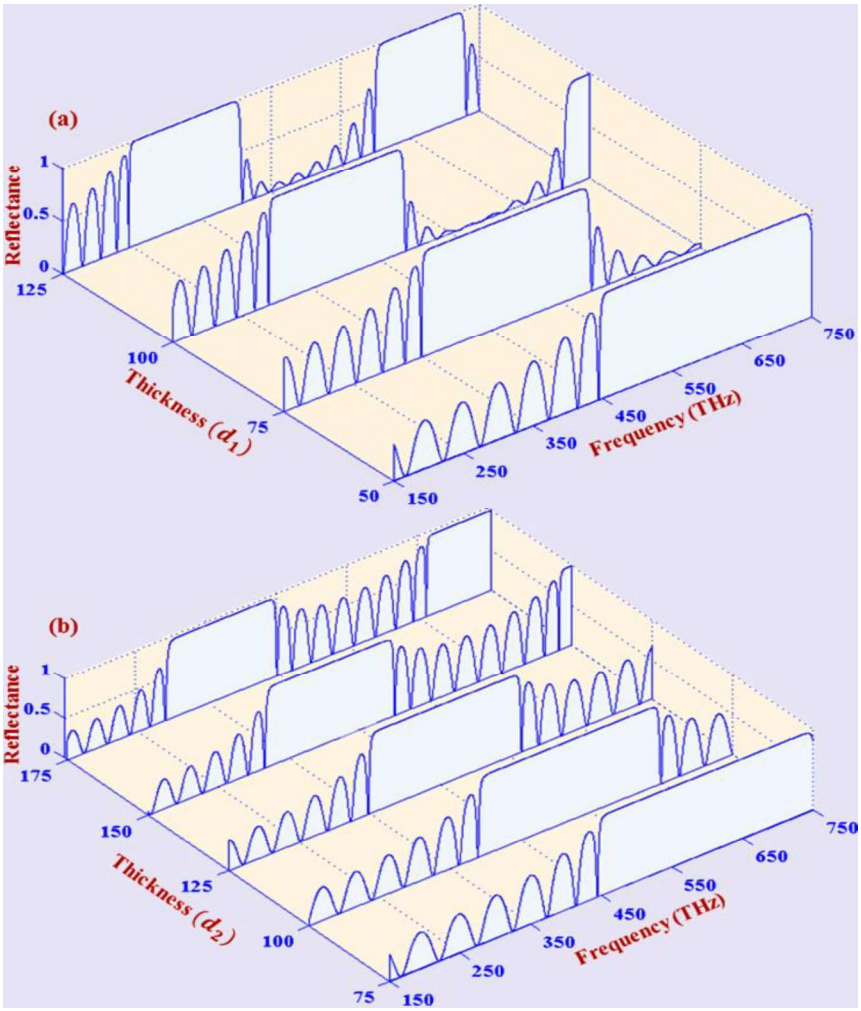

Figure 3.9 Reflectance spectra for different precise layer thicknesses of graded layers (d_1) and normal layers (d_2) for the structures with fixed values of (a) d_2 = 75 nm and (b) d_1 = 50 nm, respectively.

3.3.2 **Study of the omnidirectional band gap in the considered structures**

In this section, the Omni-directional band gap (OBG) characteristics of the proposed 1-D GPC structures with quarter-wave and latent type layer stacking arrangements have demonstrated. An OBG can be obtained within a specific frequency

range in PC as a forbidden band gap that reflects electromagnetic wave at any incident angle for both TE and TM-polarization. The dependence of the PBG on the incident angle in a quarter-wave stacked multilayer structures for TE and TM polarization are shown in figures 3.10(a and b) and 3.11(a and b) for refractive index n_B equal to 2.0 and 1.5, respectively. These figures are clearly demonstrated that the expansion of the bandwidth of PBG of the structures with n_B equal to 2.0 and 1.5 for both TE and TM-wave, when the incident angle increases.

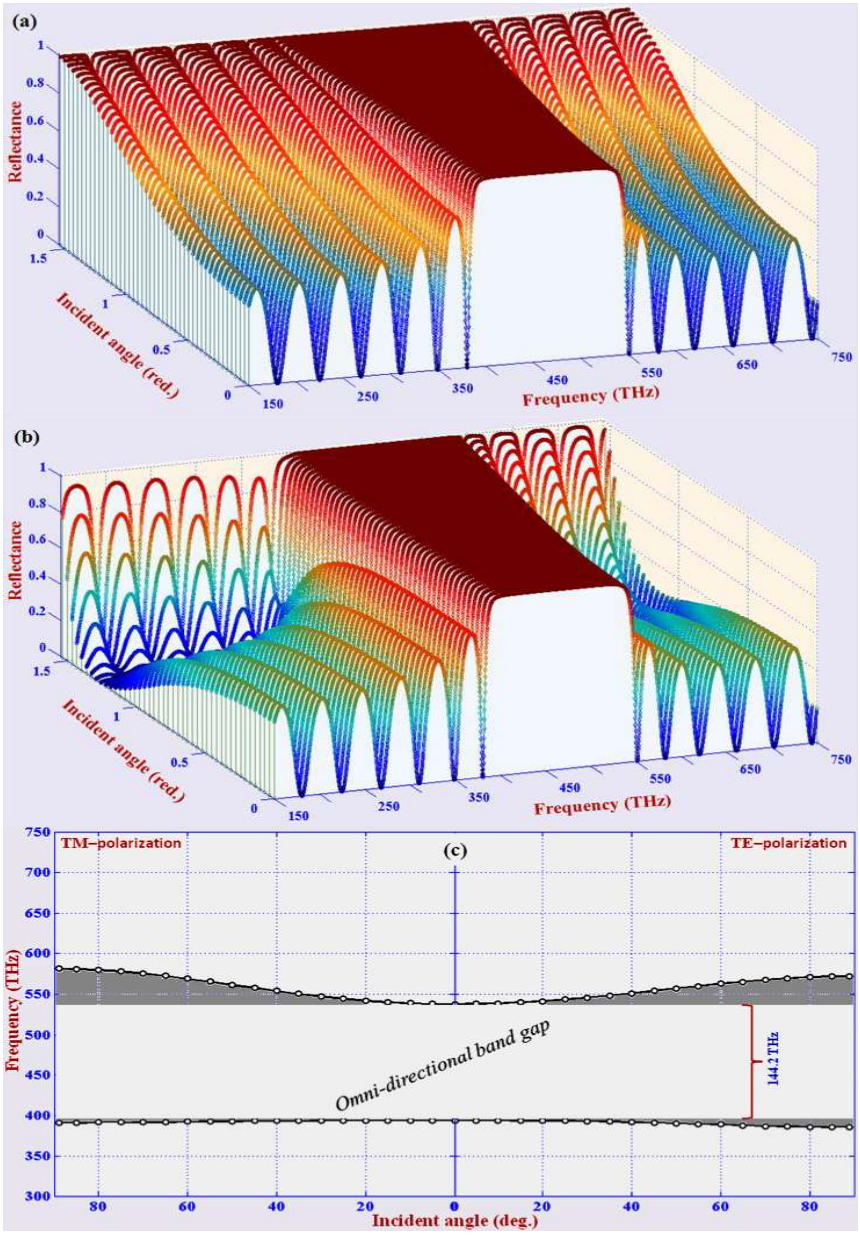

Figure 4. 10 Reflection spectra for (a) TE-polarization, (b) TM-polarization and (c) projected band spectra as changing of the incident angle of the quarter-wave stacked structure with n_B= 2.0.

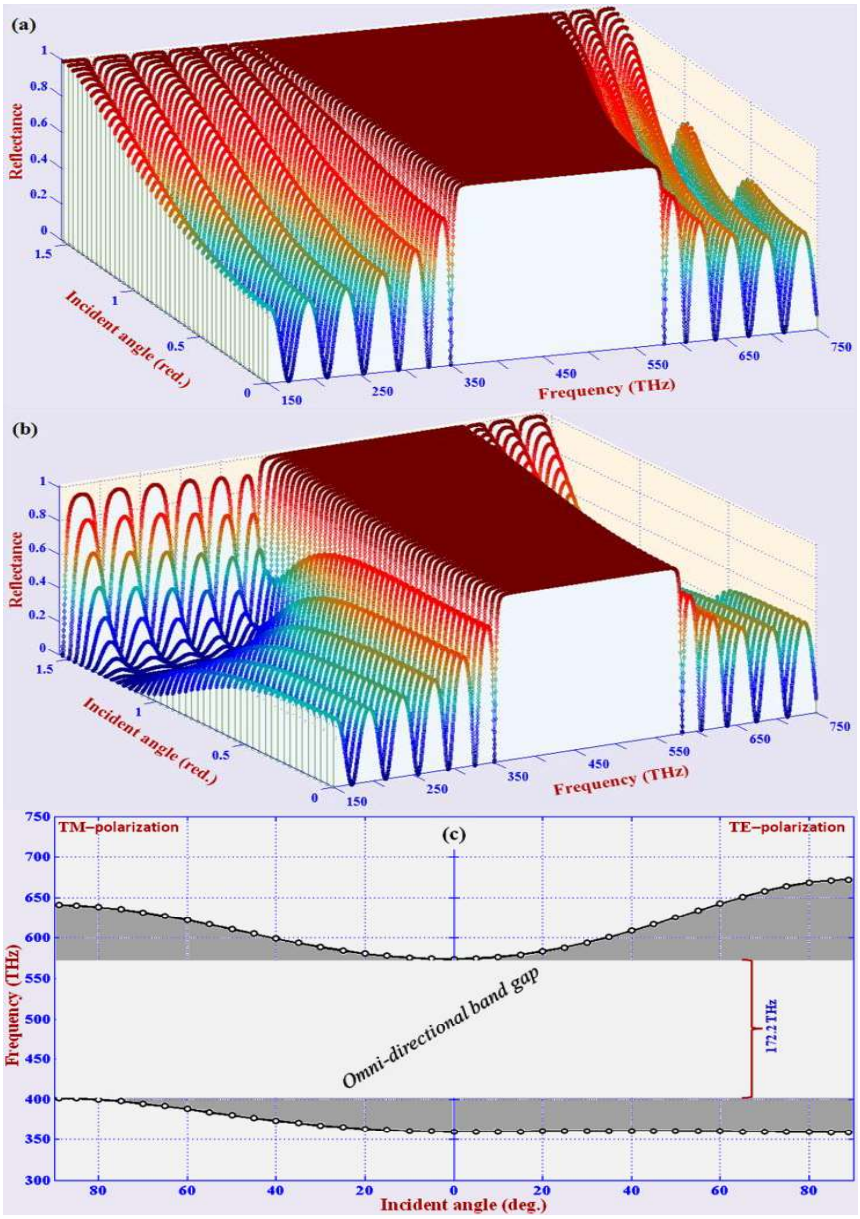

Figure 4. 11 Reflection spectra for (a) TE-polarization, (b) TM-polarization and (c) projected band structure as the changing of the incident angle of the quarter-wave structure with $\boldsymbol{n_B}$= 1.5.

In order to discuss the Omni-directional band gap properties of the structures, the projection band structures as changing of the incident angle have plotted and exhibited in figures 3.10(c), and 3.11(c), respectively for the structures with n_B equal to 2.0 and 1.5. From these figures, we can clearly inspect the variation of higher and lower band edges as changing of the incident angle. There is an OBG, which exists between higher and lower band edges as prevalent band region for both TE and TM-polarization. The photonic band spectra of the structures can be usually achieved from the projection of unit reflectance from figures 3.10(a and b) and 3.11(a and b), and OBG clearly

demonstrated from figures 3.10(c), and 3.11(c). In figures 3.10(c) and 3.11(c), the grey areas represent the forbidden band for relative polarization and the ubiquitous white area between the band edges in both polarizations illustrates the OBG. The omnidirectional bands range and bandwidths for structures with different n_B-values are tabulated in Table 3.2. It is certified from the above figures and table, an omnidirectional band exists for structure with n_B equal to 2.0 and 1.5, while it is not observed for structure with n_B equal to 1.0. But one obvious feature of this structure is that there exist broadest complete band gap for TE-wave. Therefore, the structure with n_B equal to 1.0 is more suitable for designing TE-polarized photonic devices while the structures with n_B equal to 2.0 and 1.5 can be used for to design Omni-directional photonic devices.

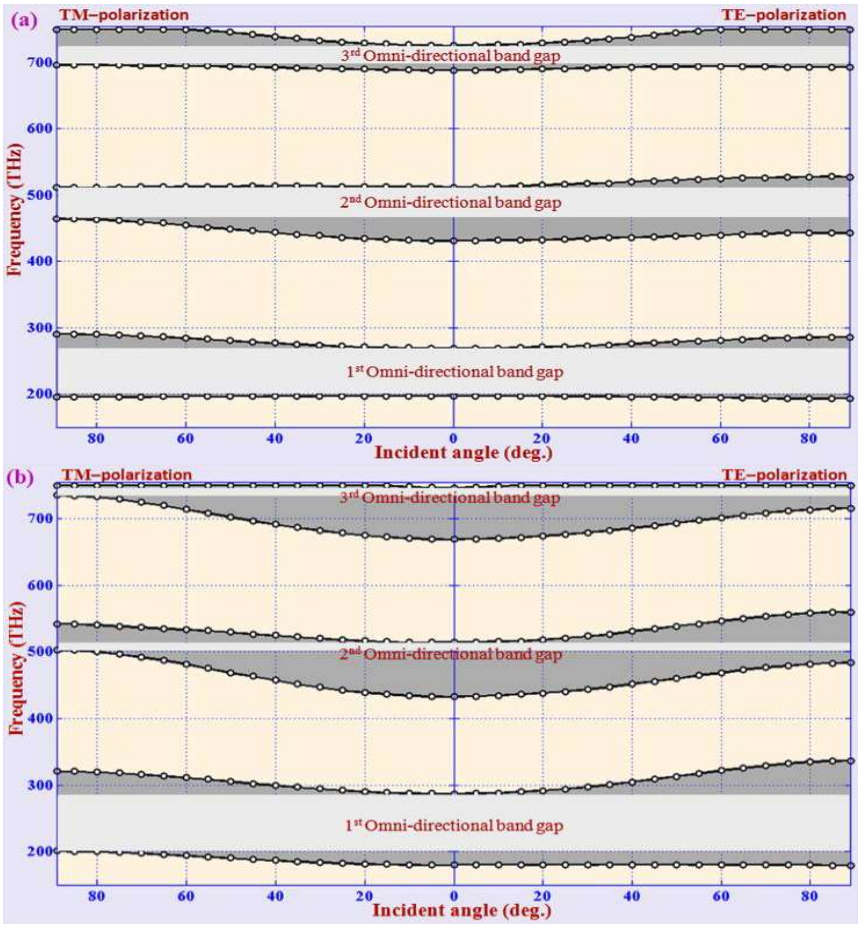

Figure 3.12 Projected band spectra as the changing of the incident angle of the latent type structures for the refractive index (a) n_B = 2.0 and (b) n_B = 1.5.

Furthermore, we have emphasized the projection band structure as the changing of the incident angle for latent type layer stacking multilayer structures with n_B = 2.0 and 1.5 and shown in the figures 3.12(a) and 3.12(b), respectively. The Omni-directional

bands range and bandwidths of such structures with different n_B-values are listed in Table 3.2. It is clear from the figure and table, as like a quarter-wave stacking structures, OBG is obtained for the structures with n_B equal to 2.0 and 1.5, and it is absence for the structures with n_B equal to 1.0. This implies that occurrence of omnidirectional bands is affected by the contrast of refractive index between constitute homogeneous and graded layer in the structures. The number of omnidirectional bands existed for the structures with n_B equal to 2.0 and 1.5. Therefore, these types of structure can be used to design the widespread omnidirectional photonic devices.

Accordingly, the existence of OBGs in graded index-homogenous materials periodic multilayered structures requires the refractive index contrast $(n_G - n_B)$ for n_B>1. Under this condition, the broader omnidirectional band range demands high value of the refractive index contrast. In addition, the omnidirectional band gaps can be adjusted by the modifying the layers thickness.

Table 3.2 Omni-directional bands region and bandwidths in the considered 1-D GPC structures for various n_B-values.

Structures with	Layer thickness constant (D)	Complete Band Region in		Omni-directional Band Region (nm)	Omni-directional Bandwidth (nm)
		TE-Polarization (nm)	TM-Polarization (nm)		
$n_B = 2.0$	$\lambda_0/4$	538.0 – 393.8	538.0 – 393.8	538.0 – 393.8	144.2
	$\lambda_0/2$	269.0 – 197.0	269.0 – 197.0	269.0 – 197.0	72
		512.2 – 443.0	512.2 – 464.6	512.2 – 464.6	47.6
		725.8 – 694.0	725.8 – 696.6	725.8 – 696.6	29.2
$n_B = 1.5$	$\lambda_0/4$	574.0 – 360.2	574.0 – 401.8	574.0 – 401.8	172.2
	$\lambda_0/2$	287.0 –180.2	287.0 –201.0	287.0 –201.0	86
		514.0 – 483.6	514.0 – 502.6	514.0 – 502.6	11.4
		746.2 – 715.6	746.2 – 735.4	746.2 – 735.4	10.8
$n_B = 1.0$	$\lambda_0/4$	627.0 – 316.8	…….	…….	…….
	$\lambda_0/2$	313.4 – 158.4	…….	…….	…….
		…….	…….	…….	…….

Now, we have emphasized the OBGs as changing of the refractive index (n_B) of the normal layer B. To do that, we calculate the ubiquitous forbidden (stop bands) frequencies regions for both TE and TM-polarization as a function of n_B is depicted in figure 3.13 for the structures with quarter wave layer arrangements. This figure shows the distribution of forbidden (black region) and allowed (white region) frequencies as a function of the $n_B$up to 4.5. Initially, the bandwidth of OBG decreases with increasing

the value of n_B up to 3.0 and then slowly increases for the higher value of n_B as shown in figure. The bandwidth of OBG is maximum for the refractive index n_B equal to 1.5.

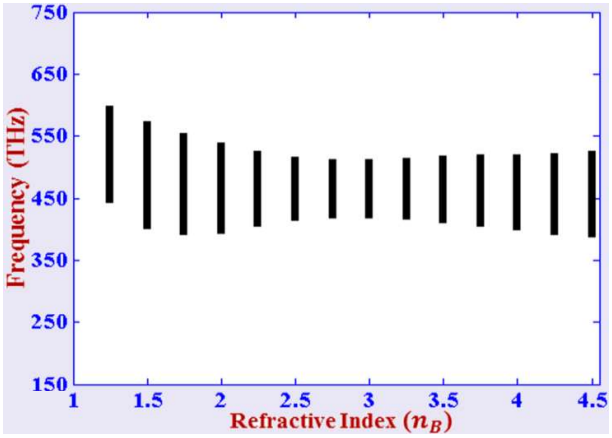

Figure 3.13 The distribution of Omni-directional band gap as a function of the refractive index n_B for the structure with quarter wave staking arrangements.

3.3.3 Effect of the ratio of n_i and n_f on the photonic band gap

Now, the dependence of the PBG on the ratio of initial and final refractive index i.e. (n_f/n_i) of the exponential graded index layer in 1-D GPC structures under normal angle of incidence has been investigated. Here, initial refractive index (n_i) is considered as a fixed value and equal to 1.5, while final refractive index (n_f) varies according to the different contrast values between them. The variations of the PBGs for different values of the refractive index ratio (n_f/n_i) are shown in figure 3.14. In the figure 3.14(a), we have depicted the refractive spectra for the various (n_f/n_i)-values in a quarter wave stacking multilayer structures with a relatively homogeneous layer refractive index n_B equal to 1.0. As expected, the photonic bandwidth decreases with decreasing the values of ratio (n_f/n_i). The explanation of this phenomenon is that the rate of modification of the grading profile parameter (γ or γ') decreases with the values of the ratio (n_f/n_i), and corresponding average refractive index over the volume of each graded layer conjointly decreases, hence influence the Bragg stack become less effectively. The PBG decreases with decreasing the grading profile parameter but that exists around the central frequency and is exhibited in figure 3.14(a). To have a more complete description and a better understanding of the effect of the ratio of initial and final refractive index of the exponential graded index layer on the PBG properties, it is important to know how that change the properties of the reflection coefficients and PBG of the considered structures for specific layer widths. In this case, we observe that the

PBG also diminishes with decreasing the grading profile parameter but here acquired band gap is shifted towards the higher frequency region, which is clearly demonstrated in figure 3.14(b). The explanation of the difference in variations of PBG in the above considered structures is that the graded layers thickness and grading profile parameter both change with the ratio of initial and final refractive index in case of quarter-wave stacking arrangements, but the thickness of graded layers are independent of the ratio of initial and final refractive index for the case of the structures with set layer widths.

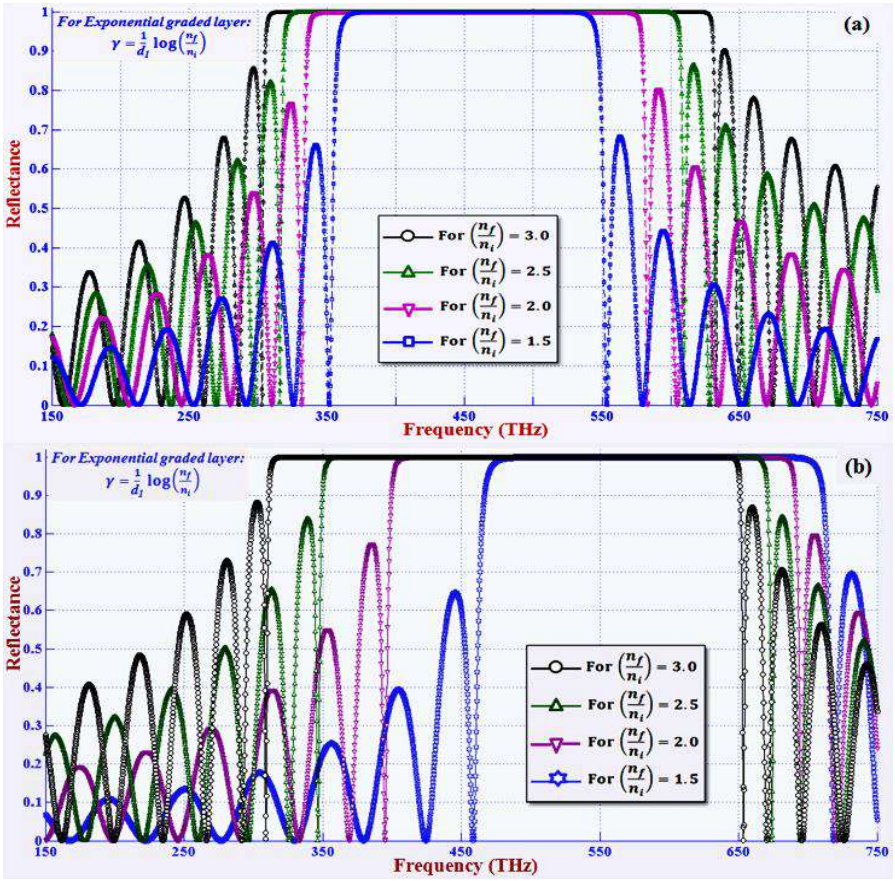

Figure 3.14 Reflectance spectra for different values of grading parameter γ (or γ') for the structures with arrangement in (a) quarter wave stacking and (b) precise layer thickness d_1 = 64 nm and d_2 = 136 nm.

Moreover, we have plotted the forbidden bandwidth by changing the ratio (n_f/n_i) for a quarter-wave stacked multilayer structure at various refractive indices of the constituted homogeneous layer under normal angle of incidence, which are depicted in the figure 3.15(a). In this figure, it can see that the photonic bandwidth decreases almost linearly for the structure with quarter-wave layer stacking arrangement. Diminishing of photonic bandwidths is observed for all values of the refractive index ratio greater or equal to the refractive index of the homogeneous layer. But, when the

values of refractive indices ratio (n_f/n_i) becomes lesser than the values of refractive index n_B than forbidden band width increases gradually which clearly revealed from third graph for n_B = 2.0 in figure 3.15(a). The photonic bands range and bandwidths at different (n_f/n_i)-values for the considered structures are tabulated in Table 3.3.

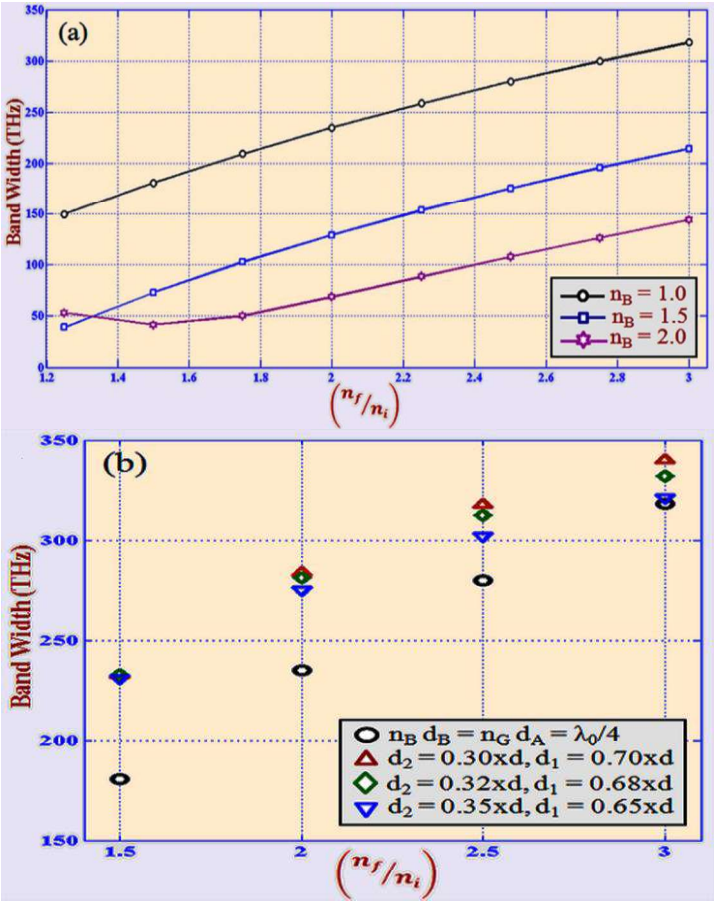

Figure 3.15 Panel (a) shows the distribution of bandwidths as a function of the ratio (n_f/n_i) for the structures with quarter wave stacking arrangement and different n_B-values and (b) exhibits the distribution of bandwidths as a function of the ratio (n_f/n_i) for the structures with specific layer thickness, and n_B= 1.0 and d = 200 nm.

Table 4.3 Reflection bands region and bandwidths in the GPC structures at normal incidence for different (n_f/n_i) values.

Ratio (n_f/n_i)	Structure with quarter-wave stacking		Structure with constant layers thickness					
			d_1 = 60 nm and d_2 = 140 nm		d_1 = 64 nm and d_2 = 136 nm		d_1 = 70 nm and d_2 = 130 nm	
	Band Range	Width	Band Range	Width	Band Range	Width	Band Range	Width
1.5	362.2-543.0	180.8	479.6-712.4	232.8	472.2-705.0	232.8	462.0-692.8	230.8
2	340.0-575.0	235	412.2-695.8	283.6	404.6-685.6	281	394.4-669.2	274.8
2.5	322.8-602.8	280	361.6-679.4	317.8	354.2-666.6	312.4	344.4-646.2	301.8
3	309.0-627.0	318	322.4-662.6	340.2	315.4-647.4	332	305.8-626.8	321

3.3.4 Photonic band gap and defect mode in one-dimensional photonic crystal with defect layer of exponential graded index material

Now, numerical results to characterize the PBG properties and defect modes due to defect layer of the exponential graded index material in the 1-D PC structures $(AB)^P ADA(BA)^P$ have presented. Superscript P represents the periodicity of the unit cells. Medium A and B are considered as a homogeneous dielectric layer of refractive index equal to 1.5 and 4.5, respectively. Medium D is considered as a defect layer having exponential grading index profile. Exponential grading profiles are considered as varying refractive index with the depth of graded layer in increasing fashion between lower refractive index (n_i) and higher refractive index (n_f) equal to 1.5 and 4.5, respectively. The refractive indices of homogeneous and graded index materials are assumed to maintain the large refractive index contrast for better appearances of grading effect on the PBG and defect modes. The enumerable number of materials is available whose refractive index exists between the above considered refractive index. In this study, we have assumed that light incident through the air medium and layered materials are a lossless dielectric. Analysis is carried out mainly in two parts. Firstly, the influences of defect layer parameters on the transmission spectra and defect modes have studied. Moreover, distributions of the electric field in such structure are computed. Secondly, the effect of incident angles on the transmission spectra and defect modes of the structure for TE and TM-polarization have been investigated. The changing in defect mode frequency and intensity as a function of incident angle is also analysed.

As mentioned above, the arrangement of the layers has been taken in the form of $(AB)^P(ADA)(BA)^P$. Defect layer D represents a layer with exponentially varying refractive index between initial (n_i) and final (n_f) refractive index as a function of the depth of graded layer. The transmission spectra of the structures without and with exponential graded index defect layer for different periodicity P are shown in figures 3.16. Thickness of the layer A, B and D are chosen in terms of quarter wave stacking arrangement as $n_A a = n_B b = n_m d = \lambda_0/4$, where a, b and d are the thickness of layer A, B and D, respectively and n_m is the mean value of the initial (n_i) and final (n_f) refractive index of the graded layer. Such types of structures are very useful and suitable for designing various photonic devices because they provide wider PBG and symmetrical reflection spectra around the centre frequency. The physical parameters used here are $n_A = 1.5, n_B = 4.5, n_m = 2.5$ and λ_0 (600 nm) is the mean value of the

considered frequency region (200 – 800 THz). The transmission spectrum of the mirror symmetry structure of the form $(AB)^6AA(BA)^6$ is shown in panel (a) and the transmission spectra of the structure to compose of a defect layer of exponential graded index material in the form $(AB)^PADA(BA)^P$ for period (P) equal to 6 and 7 are shown in panel (b) and (c) of the figure 3.16, respectively. These figures show that there exist single defect mode for the structure without defect layer and two defect modes in the forbidden band gaps for the structure with defect layer of graded index material. The defect mode of the structure without defect layer exists at the central frequency (500 THz) of considered frequency range, while in the case of structure with graded index defect layer, first and second defect modes exist at lower and higher frequency side to the central frequency, respectively.

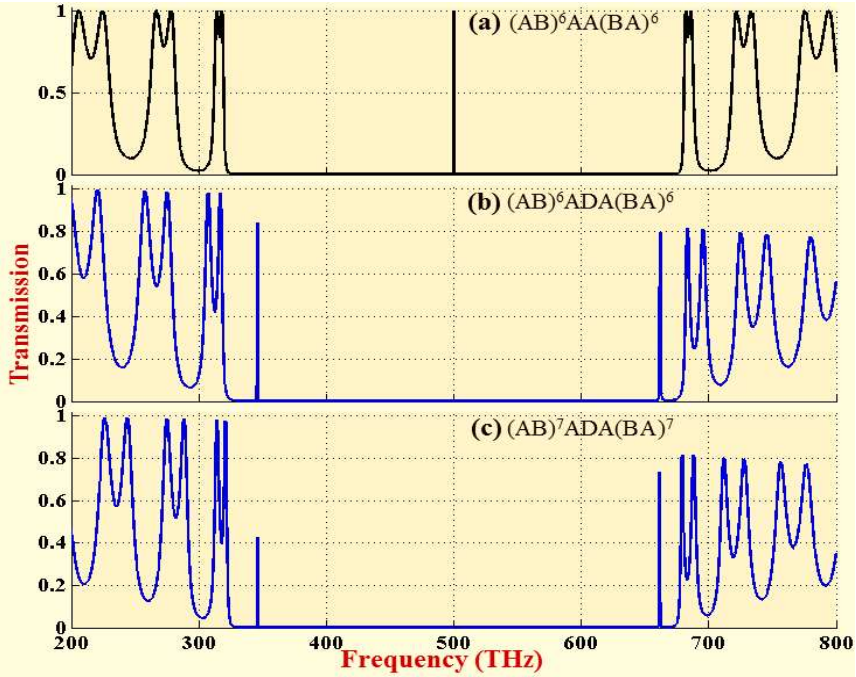

Figure 3.16 Transmission spectra of the structure (a) $(AB)^6AA(BA)^6$, (b) $(AB)^6ADA(BA)^6$ and (c) $(AB)^7ADA(BA)^7$ with exponential graded index defect layer as D. Here, refractive indices; $\boldsymbol{n_A = 1.5}$, $\boldsymbol{n_B = 4.5}$, $\boldsymbol{n_i = 1.5}$ and $\boldsymbol{n_f = 4.5}$, and thickness: $[\boldsymbol{n_A.a = n_B.b = n_m.d = \lambda_0/4}]$, where λ_0 = 600 nm and $\boldsymbol{n_m = (n_i + n_f)/2}$.

The position of first defect modes is slightly shifted toward higher frequency while position of second defect mode shifted toward lower frequency with increasing the periods. The defect mode intensities also change with periodicity. For better understanding the effect of periodicity (P) of unit cells on the defect modes frequency (f_D) and defect mode intensity, we have demonstrated the dependence of defect mode frequency (f_D) and defect mode intensity as a function of the period P in the figure 3.17.

The defect mode frequencies of the first and second defect mode slightly change the position with increasing the periodicity as depicted in panels (i) and (ii) of the figure 3.17(a). The changing of defect mode frequencies with increasing the period P become smaller and smaller. We observe that the intensity of defect modes also decreases with increasing the period P as shown in figure 3.17(b).

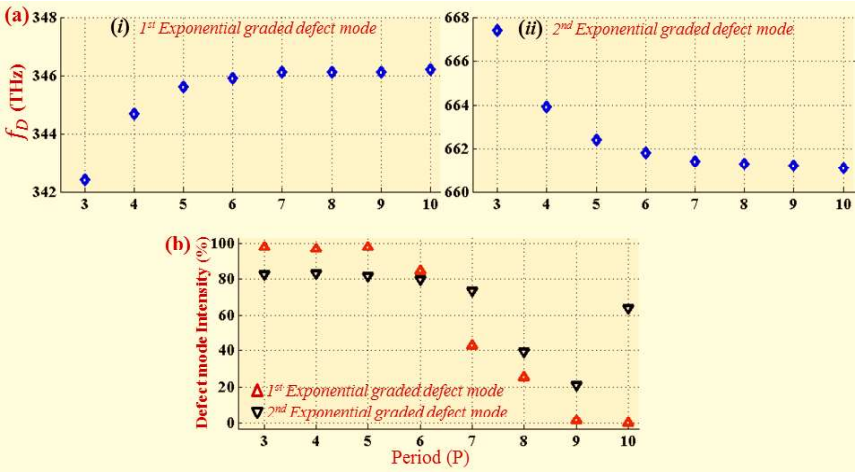

Figure 3.17 The dependence of (a) defect mode frequency (f_D) and (b) defect mode intensity on the period (P) in the structure of the form $(AB)^P ADA(BA)^P$ containing exponential graded index material as defect layer D.

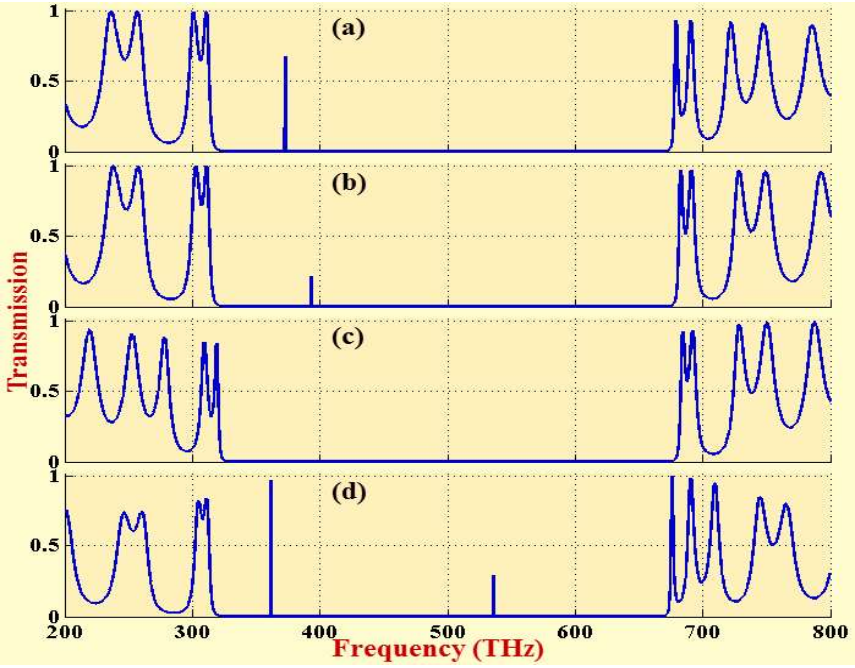

Figure 3.18 Transmission spectra of the structure of the form $(AB)^5 ADA(BA)^5$ at different thickness of exponential graded index defect layer D. The refractive indices: $n_A = 1.5$, $n_A = 4.5$, $n_i = 1.5$ and $n_f = 4.5$. Case of (a) thickness of defect layer D equal to thickness of layer B, (b) thickness of defect layer D = 25 nm, (c) thickness of defect layer D = 100 nm and (d) thickness of defect layer D = 200 nm.

With changing the thickness of graded layers, the rate of change of the relative refractive index changes and wave impedance of the graded layer also differ. The modified wave impedance of the graded layers affects the intensity of the defect modes effectively. On the other hand, the effective refractive index changes by the cause of the change of layer thickness and hence, there is a change in the optical path length. The change makes a shift of the position of the defect modes and formation of the defect modes. As is evidence from the results shown in figure 3.18, the generation of defect modes affected by the thickness of defect layer. Single defect mode exists in forbidden band gap for the defect layer thickness equal to thickness of layer B and d/2, and defect mode is absence in such structure for the defect layer thickness equal to 2d, and two defect mode form in the forbidden band gap of the structures with the defect layer thickness equal to 4d, as shown in the panel (a), (b), (c) and (d) of the figure 3.18, respectively. Considered defect layer thickness d is equal to $\lambda_0/4n_m$. Accordingly, the generation of defect modes, defect mode frequency, and normalized mode intensity can be changed by changing the thickness of graded defect layer.

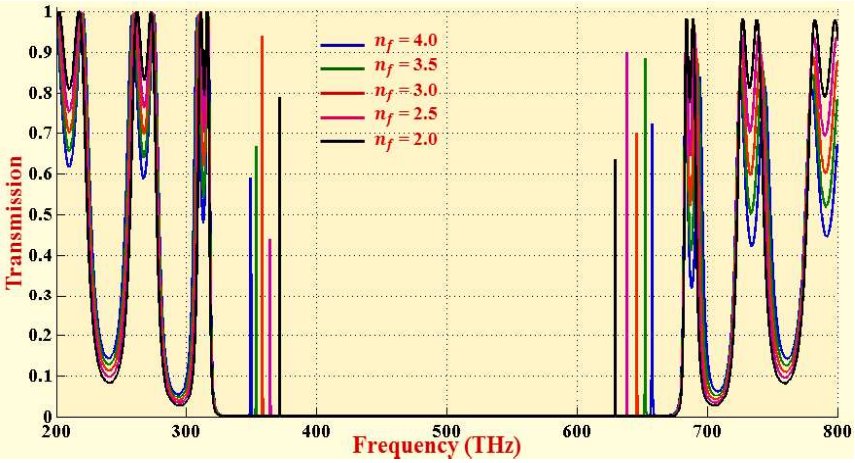

Figure 3.19 Transmission spectra at different values of contrast between initial ($\boldsymbol{n_i}$) and final ($\boldsymbol{n_f}$) refractive index of the exponential graded index defect layer of the structure $(AB)^6ADA(BA)^6$ with quarter-wave stacking arrangement. Refractive index, $\boldsymbol{n_i} = \mathbf{1.5}$, and values of $\boldsymbol{n_f}$ are shown in the figure.

Likewise, the effect gradation parameters on the photonic defect modes of the quarter-wave stacked structures $(AB)^6ADA(BA)^6$ with exponential graded index defect layer is shown in figure 3.19. Here, we have considered the initial refractive index (n_i) is fixed and equal to 1.5, while final refractive index (n_f) varies according to different contrast values between n_i and n_f. As expected, defect modes frequency of both first and second defect modes are shifted toward central frequency and defect modes

intensity also change with changing the values of contrast between the initial and final refractive index of the graded layer, but forbidden band is unaffected by the contrast values of n_i and n_f. Due to decreasing the contrast values, the rate of change of the grading profile parameter (γ) decreases and corresponding average refractive index of the volume of each graded layer also decrease, hence influence the Bragg stack become less efficiently. Hence, according to above observed results, the frequency and intensity of the defect modes can be modulated by adjusting the grading profile parameters.

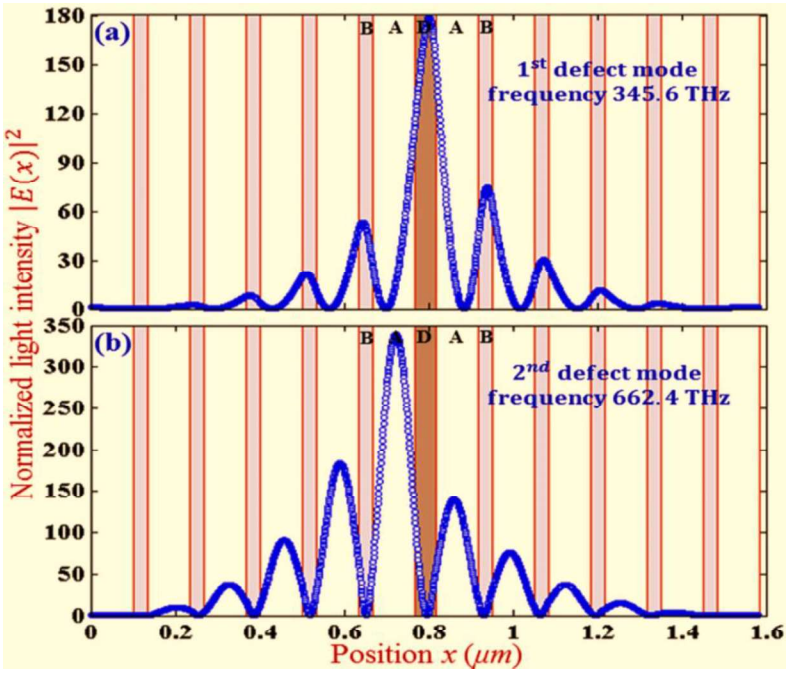

Figure 3.20 The electric field distribution at the defect modes frequency (a) 345.6 THz and (b) 662.4 THz in the structure of the form $(AB)^5ADA(BA)^5$ containing exponential graded index defect layer as D.

In the conventional PCs, it is well known that a defect mode is usually localized since strong field localization emerges inside the defect at the corresponding defect mode frequency and recognized that several potential applications in optical devices are based on field localizations [Liu (2014); Chen (2008)]. Thus, it's price of studying the field distribution inside PC structures containing linear graded index defect. In figure 3.20, the numerical simulations of the field distributions of the structure of the form $(AB)^5ADA(BA)^5$ containing a defect layer of exponential graded index material as D have demonstrated. Strong localizations are found at the frequency of the defect modes, and defect modes frequencies are 345.6 THz and 662.4 THz, which can obtain from the transmittance spectra of the structure of the form $(AB)^5ADA(BA)^5$. It can see that the electric field corresponding to first defect mode at frequency 345.6 THz is mainly

localized in defect layer D as shown in figure 3.20(a). On the other hand, the electric field corresponding to second defect mode at frequency 662.4 THz is mainly localized in central layer A as depicted in figure 3.20(b). Therefore, the coupling layers A and D are behaving two different kinds of effective defects and relate to the corresponding defect states at interface boundary of the graded defect layer D. The characteristics of electric field distribution lead to the change of defect modes frequency and intensity.

Now, the influence of incident angle on the defect modes for TE and TM-polarization in the structure $(AB)^6ADA(BA)^6$ with exponential graded index defect layer have investigate. We have assumed that the structural parameters are same as above. The dependence of transmittance on the incident angle for TE-mode and TM-mode is shown in figure 3.21(a - e) and 3.22(a - e) respectively corresponding to the incident angles from 0^o to 60^o with an interval of 15^o.

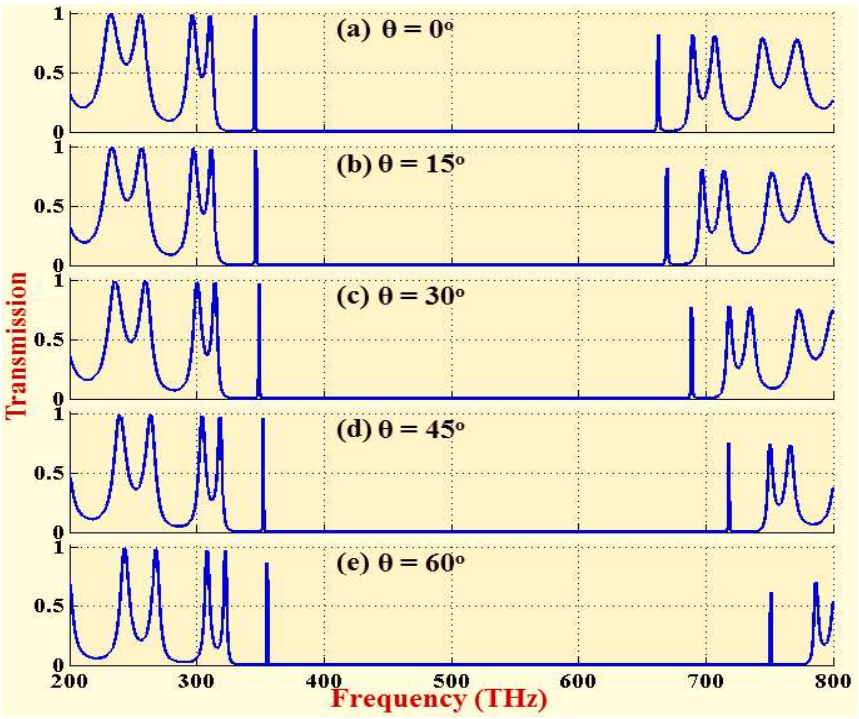

Figure 3.21 Transmission spectra at different incident angle (a) $\theta = 0^o$, (b) $\theta = 15^o$, (c) $\theta = 30^o$, (d) $\theta = 45^o$ and (e) $\theta = 60^o$ for TE-wave of the structure $(AB)^6ADA(BA)^6$ containing exponential graded index defect layer as D.

According to the transmission spectra, the defect modes frequency and intensity are change with the incident angle for both TE and TM-wave. It can also be seen that the defect modes of the structures are shift toward higher frequency with increasing the incident angle for both TE and TM-wave. The photonic bands for TE-wave are spreading toward the higher frequency, while which are shrinking for TM-wave but

shift toward the higher frequency, with increasing the angle of incidence. The defect mode intensities also change with the incident angle for both TE and TM-wave.

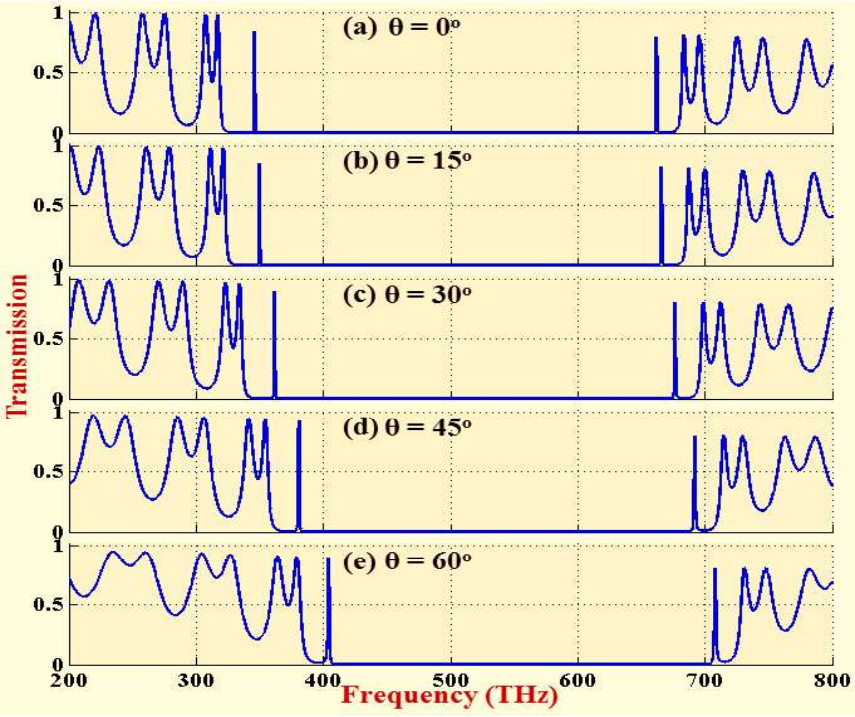

Figure 3.22 Transmission spectra at different incident angle (a) θ = 0°, (b) θ = 15°, (c) θ = 30°, (d) θ = 45° and (e) θ = 60° for TM-wave of the structure $(AB)^6ADA(BA)^6$ containing exponential graded index defect layer as D.

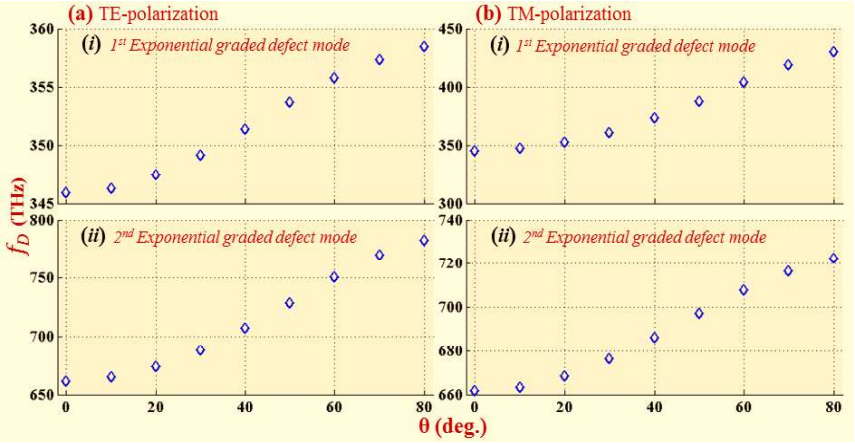

Figure 4. 12 The dependence of defect mode frequency (f_D) on the incident angle (θ) for (a) TE-mode and (b) TM-mode in the structure form of $(AB)^6ADA(BA)^6$ containing exponential graded index defect layer as D.

In order to discuss the variation of defect mode frequency (F_D) for TE and TM-wave, we have plotted the shifting frequency of the defect modes as a function of incident angle (θ) in figures 3.23(a) and 3.23(b), respectively. From these figures, the variation of the defect mode frequency of the first and second defect modes for both TE

and TM-modes as changing the incident angle can clearly inspect. The defect modes frequency is shift toward the higher frequency with the incident angle. In addition, we have demonstrated the dependence of defect mode intensity on the incident angle (θ) for TE-mode and TM-mode in figures 3.24(a) and 3.24(b), respectively. It can see that the intensities of both defect modes for TE-wave and TM-wave randomly change with increasing the incident angle. Therefore, the position and intensity of the defect modes can also modulate by changing the incident angle and polarization.

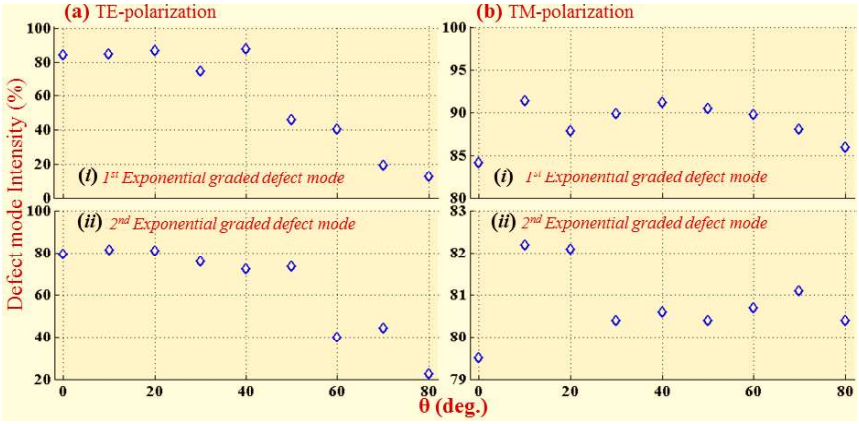

Figure 4. 13 The dependence of defect mode intensity on the incident angle (θ) for (a) TE-mode and (b) TM-mode in the structure form of $(AB)^6ADA(BA)^6$ containing exponential graded index defect layer as D.

Accordingly, the average refractive index of the graded defect layer and different grading profile parameters have significant influence on the frequency and intensity of the defect modes and field localization in the proposed structures. Hence, several structural parameters are accessible to tune the desirable defect modes in the 1-D PCs with exponential graded index defect layer.

3.4 Conclusion

In this chapter, the influences of exponential graded index materials on the photonic and omnidirectional band gap and defect mode properties of 1-D GPCs have been theoretically investigated. Initially, the tunability of the photonic and omnidirectional band gap in 1-D periodic multilayer structures constituted with an exponential graded and normal refractive index materials have demonstrated. The number of photonic band gap increases with increasing layers thickness and their bandwidths decrease as the increase of refractive index of the homogeneous layer. Bandwidths of photonic band gaps also decrease with grading parameter. The gradation profiles have a substantial influence on the reflection phase shift and electric field

distribution. In addition, the omnidirectional band gap also exists when the relative refractive index of the homogeneous layer equal to 1.5 and 2.0, but it does not exist for 1.0. Thus, 1-D GPC structures with the relative refractive index of the constituted homogeneous layer greater than 1.0 are suitable to design the widespread omnidirectional band gap devices. In the case of TE-polarization, such types of structures with the refractive index of the homogeneous layer equal to 1.0 have wide common reflection band. Therefore, these structures can be utilized especially for the configuration of TE-polarized optical devices.

Next, the tunability of defect modes in 1-D PC containing a defect layer of a gradual variation of refractive index in an exponential fashion as a function of the depth of layer has investigated. The generation, position, and intensity of defect modes are demonstrated for different structural parameters, grading parameters and angle of incidence and polarizations. The defect mode frequency and intensity strongly depend on the value of contrast between initial and final refractive index of the constituted defect layer of graded index material. The position of the defect modes shifts toward central frequency and their intensity also change with the grading parameters. In this way, the position and amplitude of the defect modes can control by adjusting the structural and geometrical parameters. The enhancement of electric field also found due to the localization of light in the defect layers. The defect mode frequencies and intensities of the defect modes can also be tuned by changing the incident angle and polarization. Thus, desired defect modes with different frequency position and intensity can be achieved by selecting appropriate structural parameters, grading parameters, angles of incidence and polarization in 1-D PC structures with defect layer of exponential graded index materials.

Accordingly, the desired tunable photonic and omnidirectional band gaps and defect modes can be achieved by selecting appropriate parameters of the proposed structures. Thus, the proposed structures can be used to design various photonic devices such as reflectors, multi-channel filters, mirror and optical sensors, etc. As similar to previous work this work also opens the field of understanding the effect of exponentially graded index materials and obtaining the desired photonic and omnidirectional band gaps and defect modes in 1-D graded photonic crystals.

★★★★★★